CHAPTER 5

SUBSURFACE RESISTIVITY RESULTS AND CORRELATION WITH GROUNDWATER QUALITY

5.1 Introduction

This chapter discusses the subsurface resistivity surveys results conducted in Carey Island. Subsurface resistivity results were correlated with groundwater chemistry data for establishing an empirical relationship. Statistical analysis was used to determine the relationship between subsurface resistivity and groundwater chemistry. This relationship is then used to determine the groundwater salinity (fresh, brackish and saline) of aquifer system in Carey Island. Time-lapse resistivity measurements were used to study salinity changes of the groundwater aquifer. The flowchart of subsurface resistivity results and the correlation with groundwater quality is shown in Figure 5.1

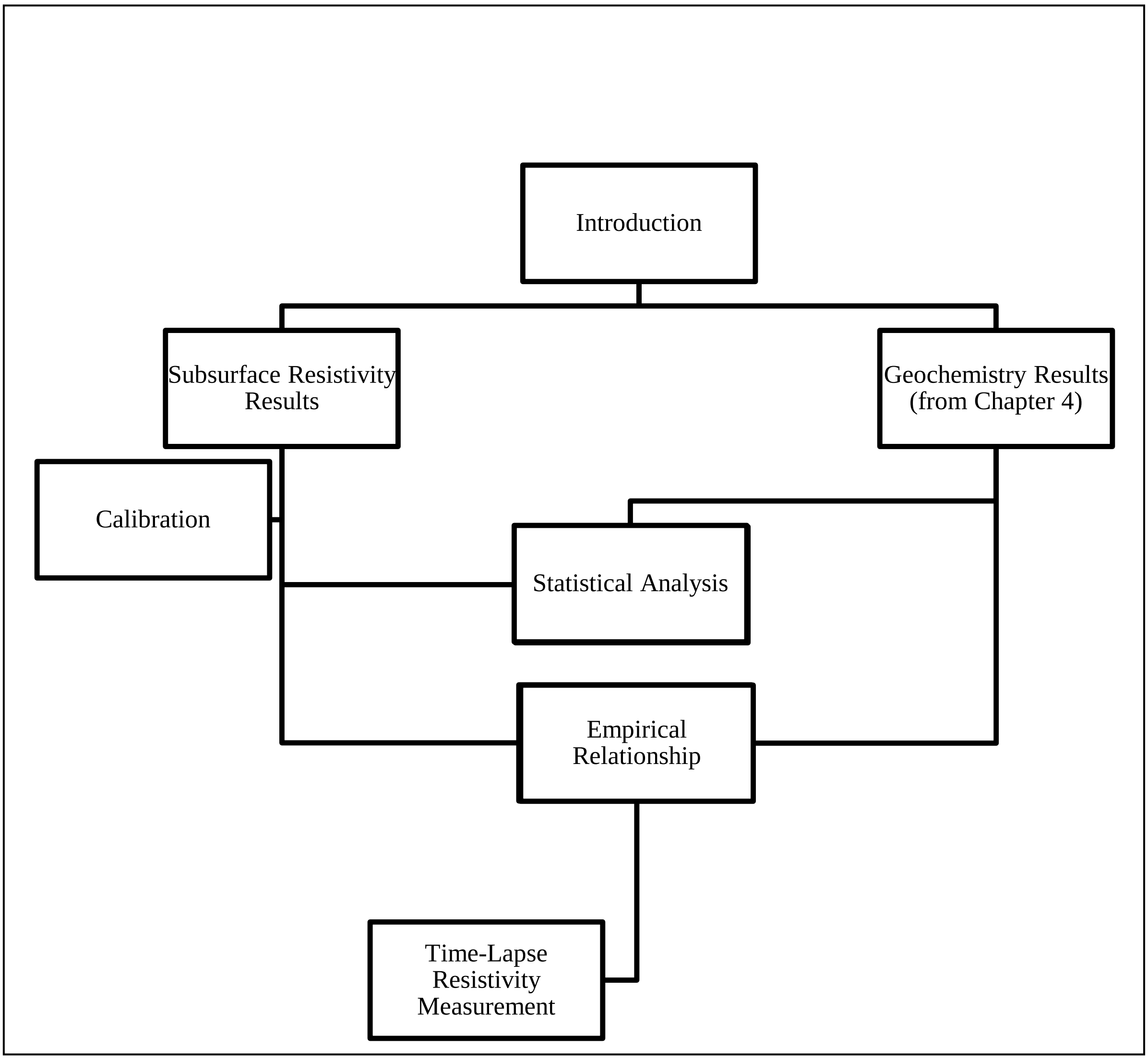

Figure 5.1: Flowchart of subsurface resistivity results and the correlation with groundwater quality

5.2 Subsurface resistivity results

The first phase of subsurface resistivity survey involved the derivation of correlation between subsurface resistivity and TDS of groundwater samples. Subsurface resistivity surveys were done three times which was in August 2009, November 2009 and February 2010. Resistivity measurements locations from eight transverse resistivity surveys over the monitoring wells are shown in Figure 5.2. In the analysis, the measured resistivity data were merely apparent and subjected to the inversion that resulted in a model of subsurface resistivity. This model represents approximately the true subsurface resistivity distribution as described by Loke (2013a). Two-dimensional (2-D) subsurface resistivity model resulting from the analysis are shown in Figures 5.3 until 5.20.

The results of resistivity images showed low resistivity (<3 Ω.m) in over 80 % of the image obtained (Figures from 5.3 to 5.8 and 5.11 to 5.18), except for MW6 (Figures 5.9 and 5.10) and MW12 (Figures from 5.19 to 5.20). Resistivity values of MW6 did not exceed 8.5 Ω.m, whereas those for MW12 ranged from 1.0 to 14.0 Ω.m.

Higher resistivity ranges have been reported for island coastal areas in other studies; for example, 0–1,000 Ω.m (Wilson et al., 2006) and 0–2,500 Ω.m (Pujari and Soni, 2008). Wilson et al., (2006) in their study on marine sand derived a formation factor from consideration of measured pore-fluid resistivity and estimated bulk resistivity, which could be used as first approximation of pore-fluid resistivity (hence determination of groundwater salinity degree) in future resistivity surveys. Resistivity value less than 5 Ω.m was interpreted to represent seawater intrusion. Pujari and Soni (2008) found a narrow resistivity band existed in an Indian coastal limestone area with resistivity from nearly 0–3.0 Ω.m, which was interpreted to represent seawater intrusion. In the local (Malaysia) studies, Nawawi et al., (2001) interpreted resistivity of less than 5 Ω.m to represent saline water in the western coast of Peninsular Malaysia; while Surip (1994) suggested resistivity less than 2 Ω.m was to represent alluvial salinity in the eastern coast.

Various underlying assumptions were used in the present study. Very low resistivity (from nearly zero to 3.0 Ω.m) was taken to represent saline water and higher resistivity (3.0–24.0 Ω.m) representing a mixture of freshwater and seawater. Since the Island's alluvial Quaternary is comprised of homogenous water-bearing sand and some gravel (due to large volumes of pore fluids), large volumes of groundwater could presumably flow through the fluid pores, thus causing resistivity to be affected more by the pore fluids rather than by the mineral soil composition, which in turn might allow the resistivity image of groundwater salinity to be more apparent.

Surface elevation in study area ranges from 1.1 to 2.3 m above mean sea level (Appendix A). The topography can be assumed almost flat (based on evidently small topographical variations <1.0 m). High groundwater tables (0.461 to 1.560 m above mean sea level) were observed (Table 5.1). The inversion subsurface resistivity model used the Wenner array configuration, by which the smallest electrode spacing selected was to be 5 m, which resulted in the resistivity image to start at the 1.50 m depth; the subsurface resistivity profile below the 1.50-m depth was taken as fully saturated with groundwater.

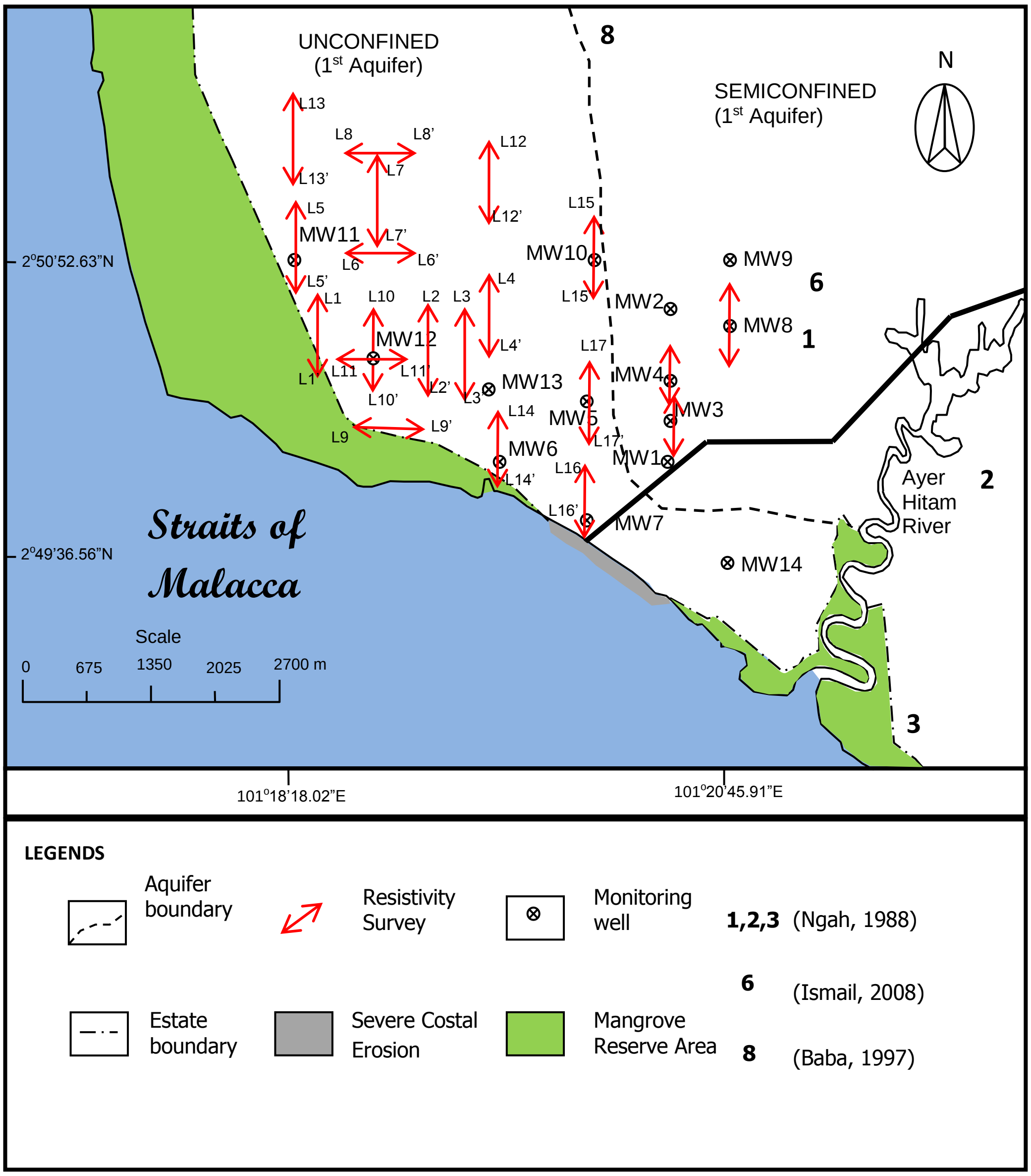

Figure 5.2: Locations of resistivity survey and monitoring wells in study area. Some of resistivity survey crossed over the monitoring wells

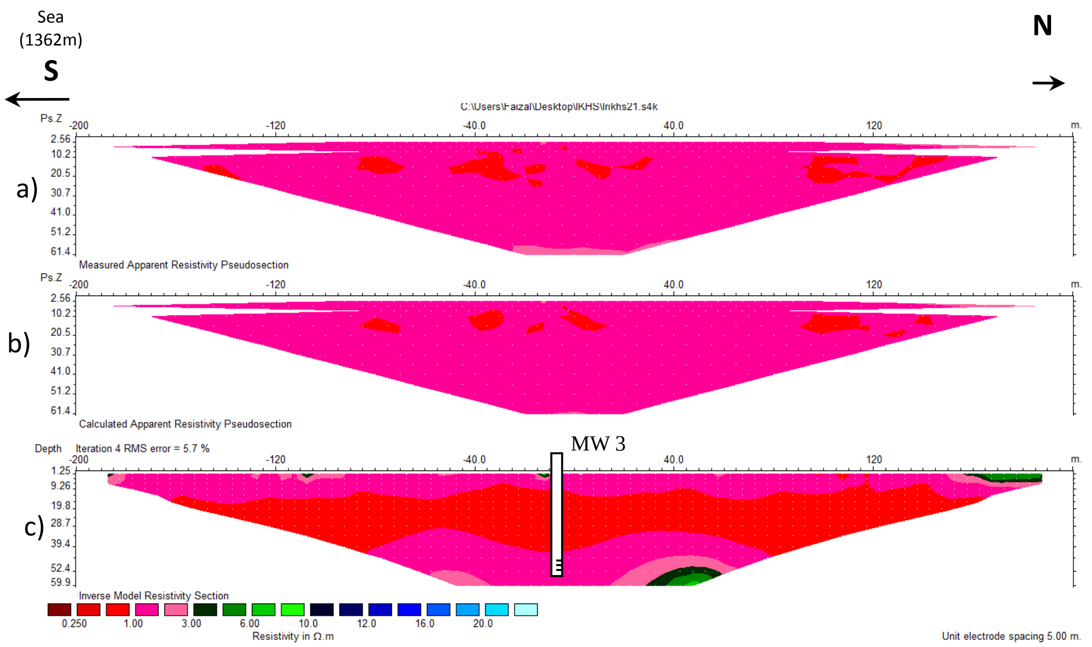

Figure 5.3: MW3 resistivity images, August 2009; a) Measured apparent resistivity (Wenner Array), b) Calculated apparent resistivity, and c) Inverse model resistivity

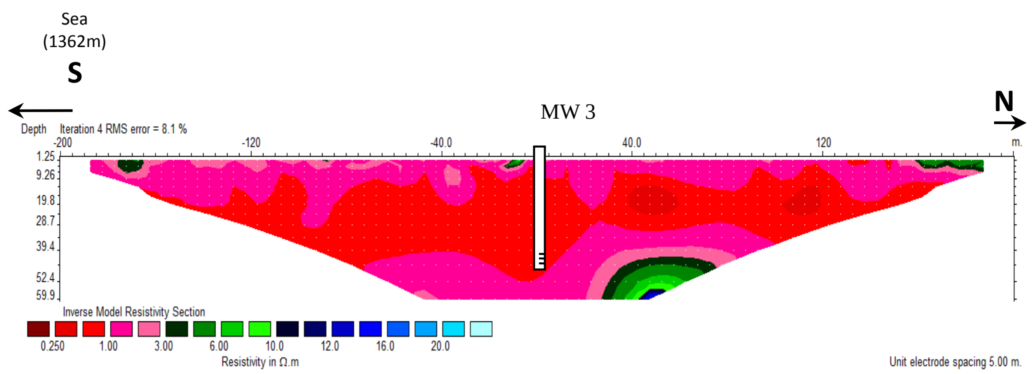

Figure 5.4: MW3 resistivity image, November 2009

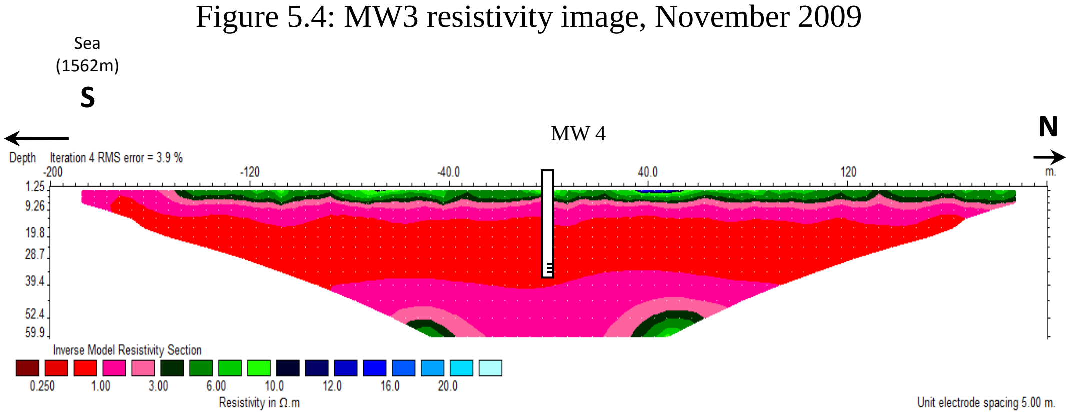

Figure 5.5: MW4 resistivity image, November 2009

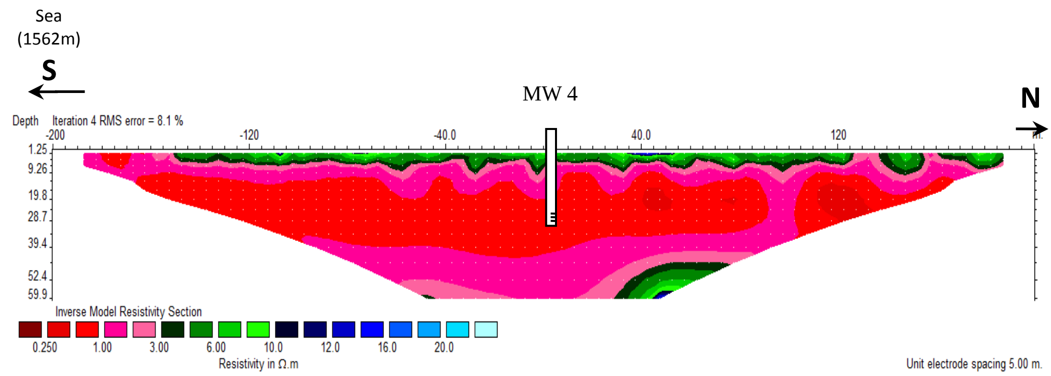

Figure 5.6: MW4 resistivity image, February 2010

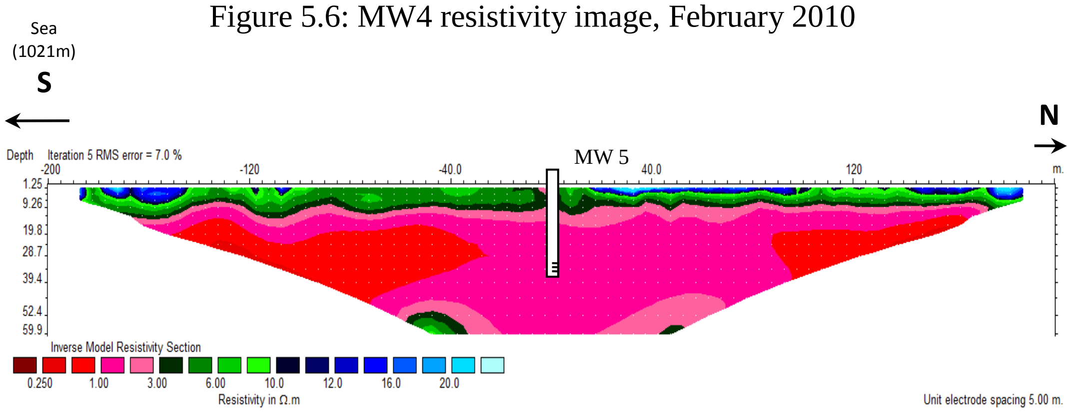

Figure 5.7: MW5 resistivity image, August 2009

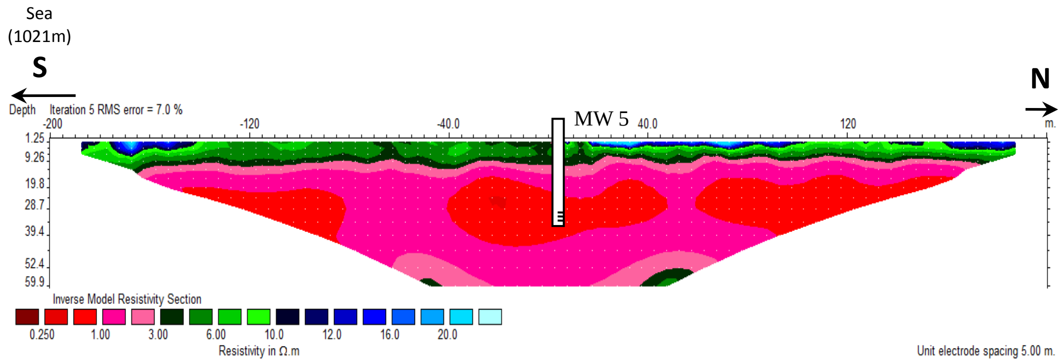

Figure 5.8: MW5 resistivity image, February 2010

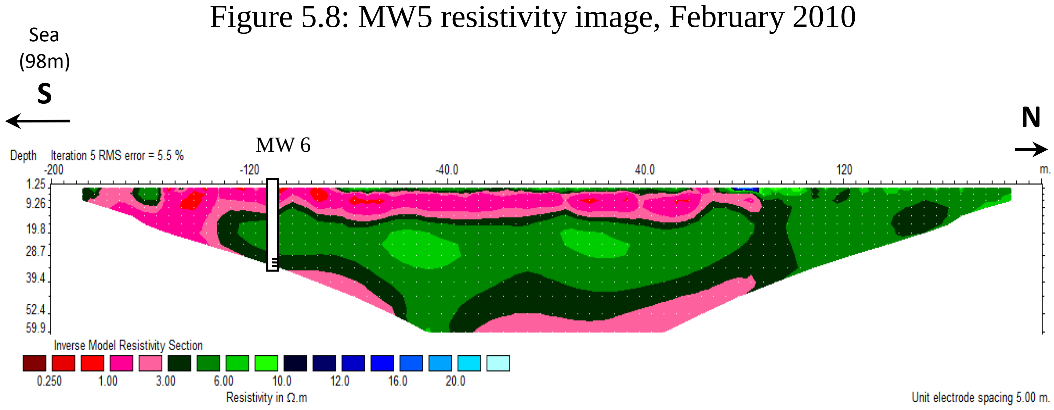

Figure 5.9: MW6 resistivity image, August 2009

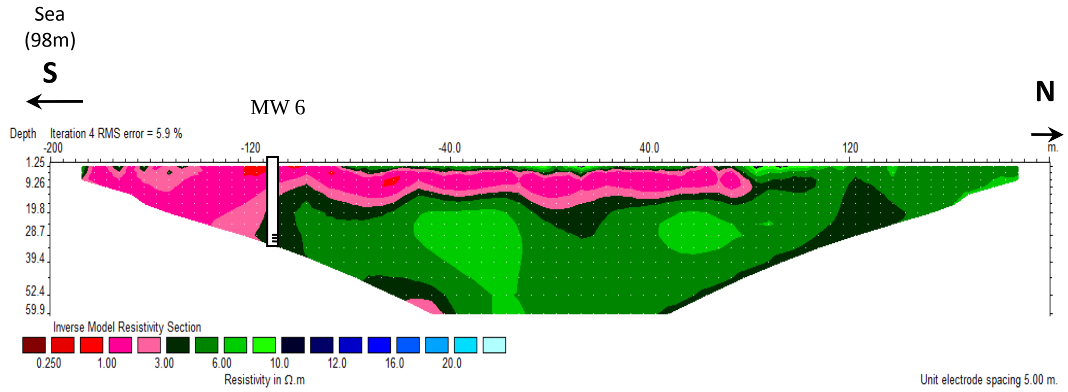

Figure 5.10: MW6 resistivity image, November 2009

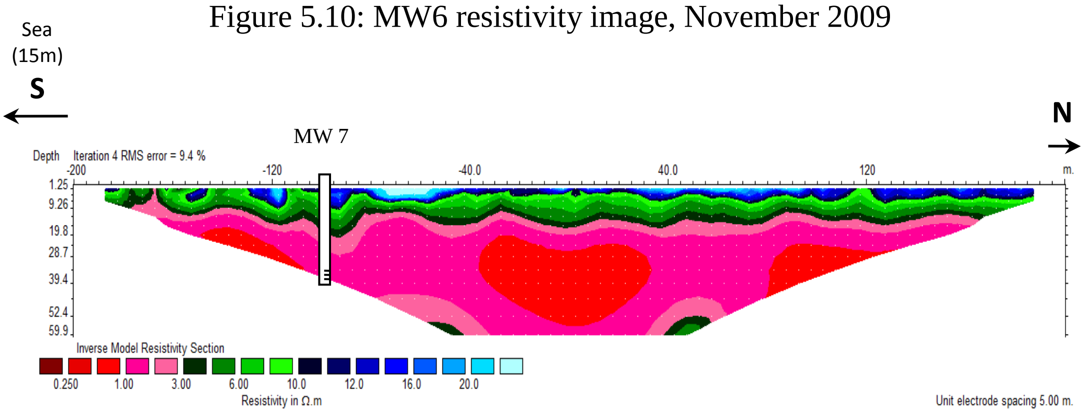

Figure 5.11: MW7 resistivity image, August 2009

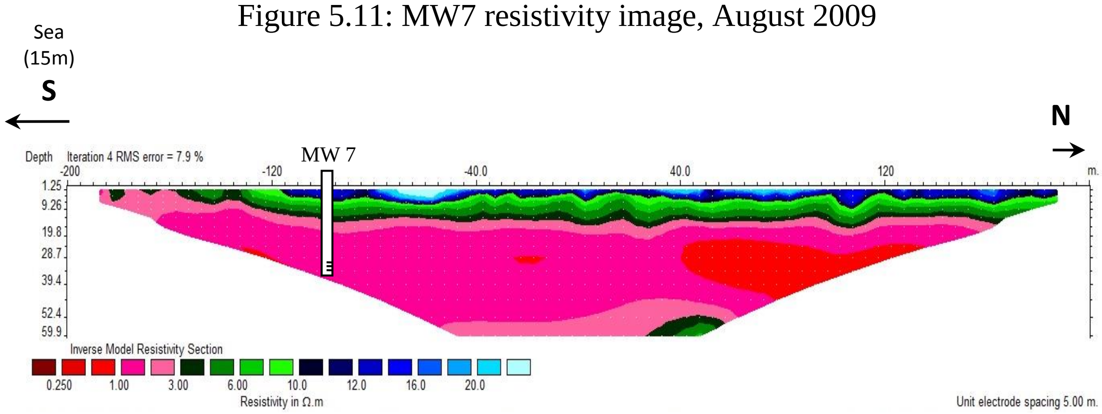

Figure 5.12: MW7 resistivity image, November 2009

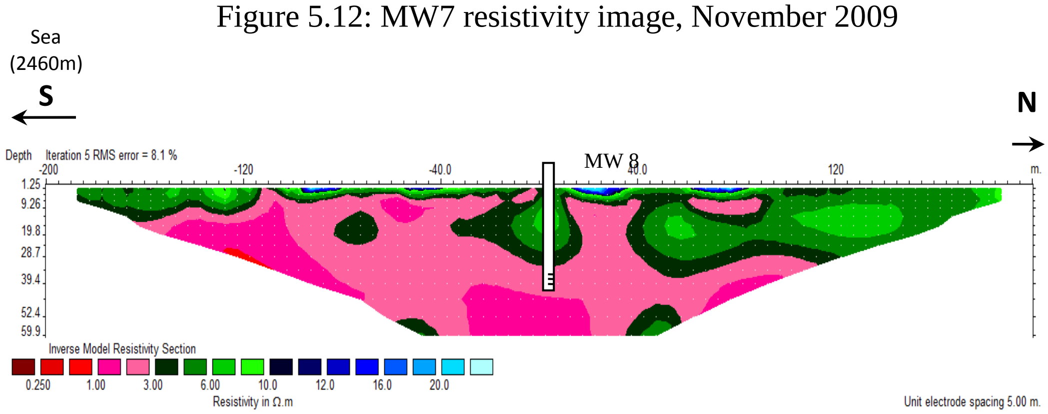

Figure 5.13: MW8 resistivity image, August 2009

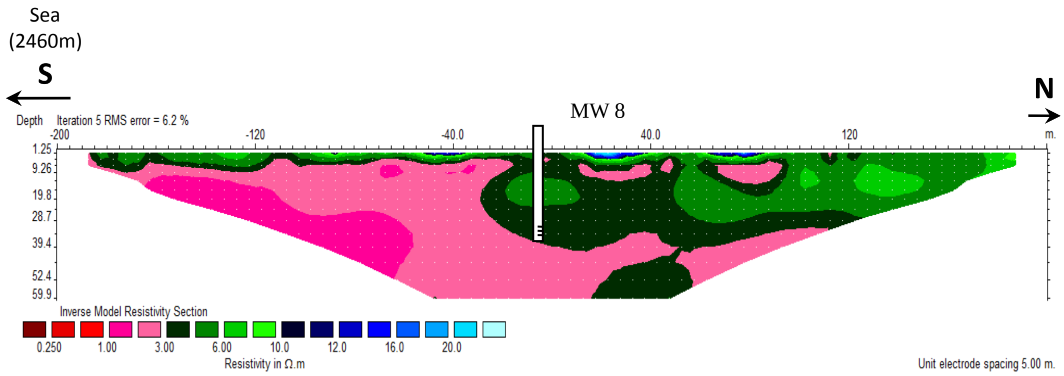

Figure 5.14: MW8 resistivity image, February 2010

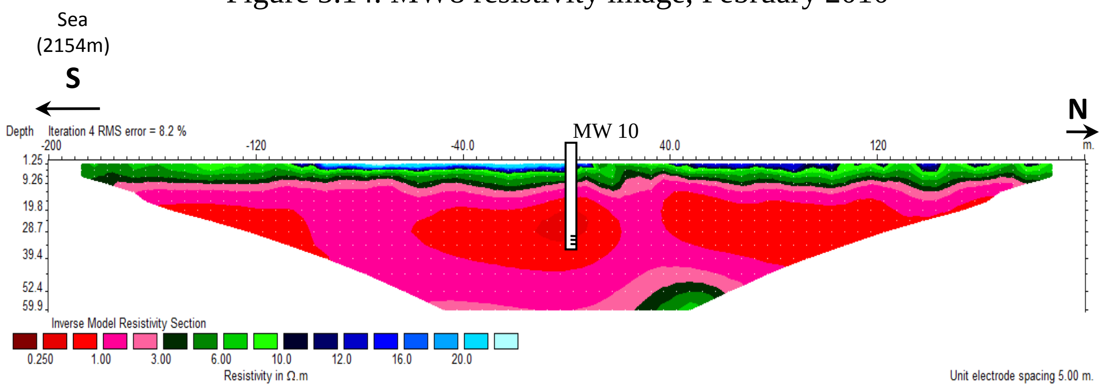

Figure 5.15: MW10 resistivity image, August 2009

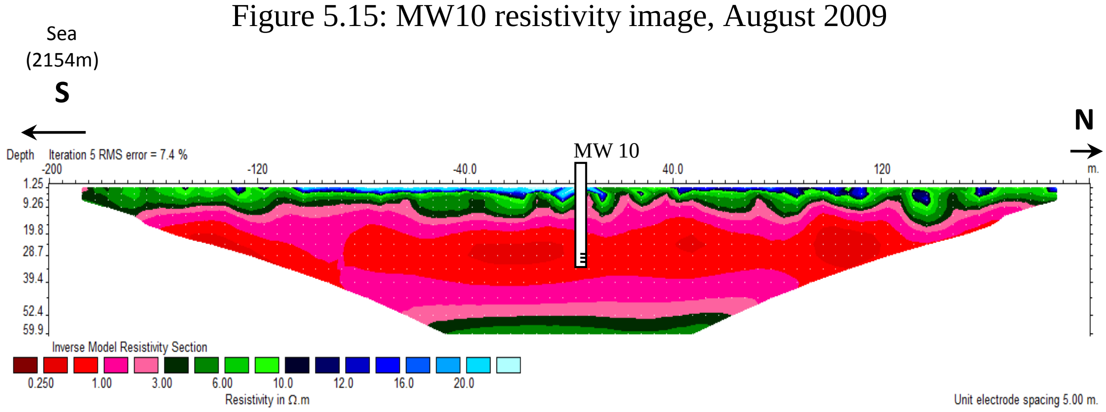

Figure 5.16: MW10 resistivity image, February 2010

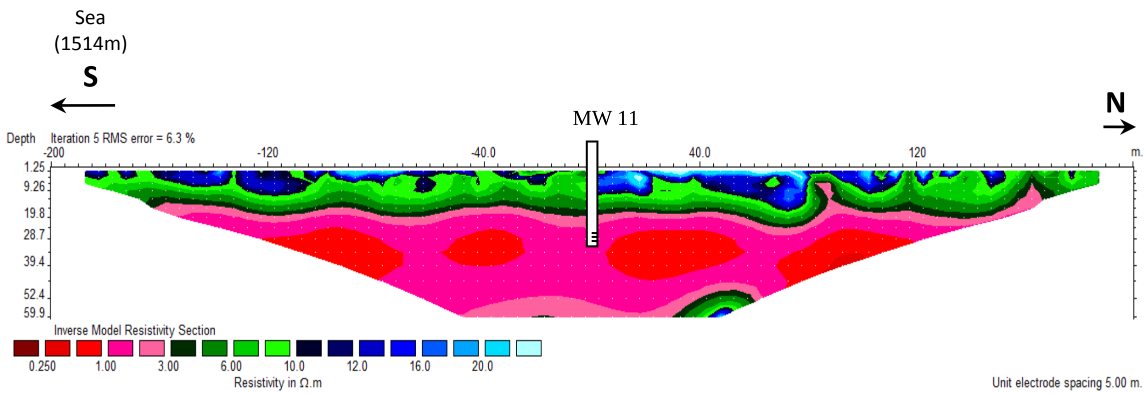

Figure 5.17: MW11 resistivity image, August 2009

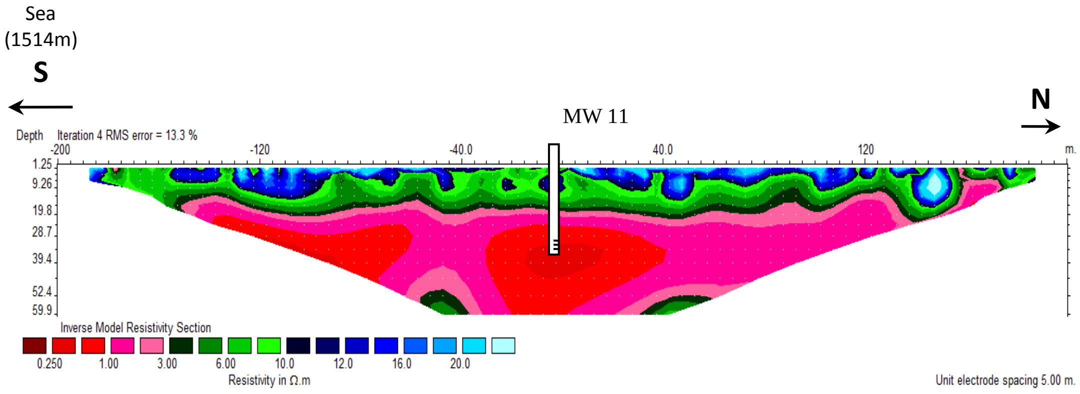

Figure 5.18: MW11 resistivity image, February 2010

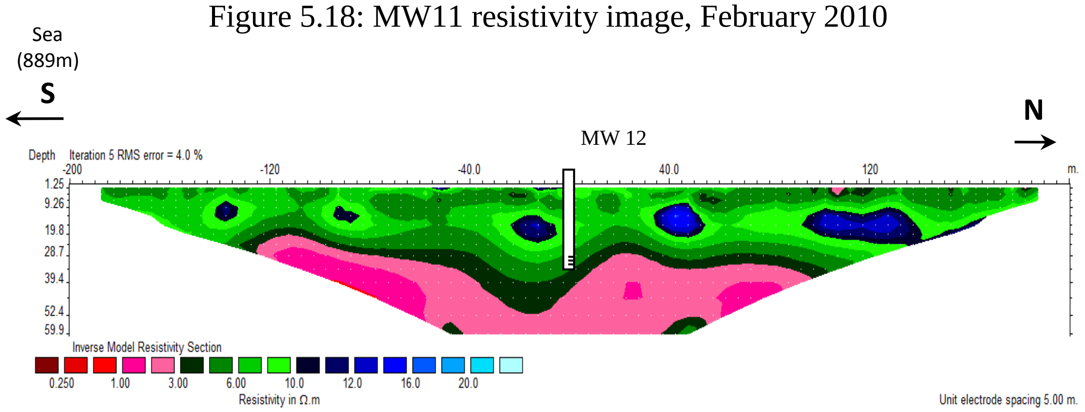

Figure 5.19: MW12 resistivity image, August 2009

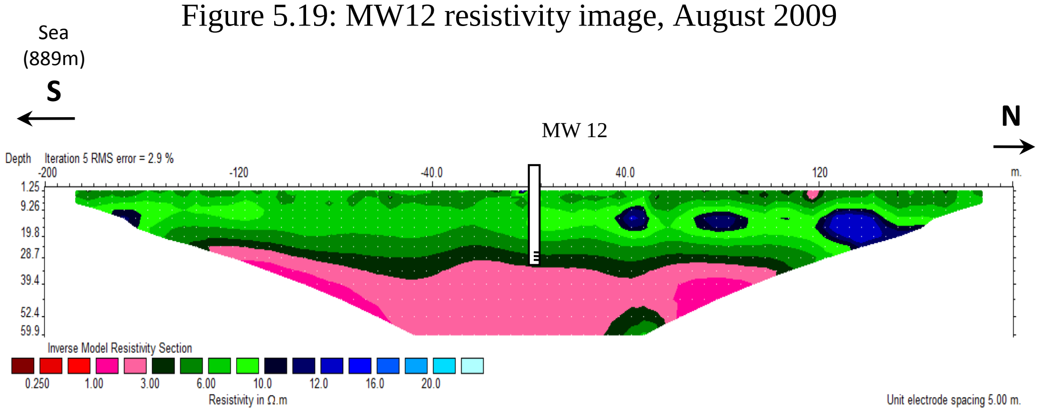

Figure 5.20: MW12 resistivity image, February 2010

5.3 Correlation between subsurface resistivity and water types

Ebraheem et al., (1997, 2012) and Sherif et al., (2006) suggested that the geophysical and geochemical data might be correlated to obtain an empirical relationship if dissolved ions were found in the pore fluids rather than in the host soil, which was important for controlling the electricity-transmitting ability of groundwater according to Sherif et al., (2006). The procedures for obtaining these relationships were as described by Cartwright and McComas (1968), Ebraheem et al., (1990, 2012) and Sherif et al., (2006). Water specific conductance was derived from reciprocals of water resistivity ($\rho_w = {}^{1}/_{\sigma_w}$) while soil conductance as the inverse of the subsurface resistivity $\left(\sigma_s = {}^{1}/_{\rho_e}\right)$.

In this study, the empirical relationship was derived using twenty three data from subsurface resistivity, water specific conductance and TDS as shown in Table 5.1. The data were collected from eight resistivity survey measurements and eight deep monitoring wells. The data was evaluated statistically using skewness, kurtosis, and Pearson correlation coefficient (r) to evaluate the distribution and correlation. Statistical analyses of the measured groundwater conductivity, resistivity, and TDS plus calculated soil conductivity and groundwater resistivity indicated the skewness and kurtosis for each data set were both within -1 to +1. This showed that the distribution of the data followed the normal distribution. A linear relationship was obtained as indicated by the Pearson correlation coefficient (r) between -0.9 and +0.9. The result indicates the data tested had linear correlation. The results of the statistical analysis are enclosed in Appendix J.

Table 5.1: Data used for empirical relationships between subsurface resistivity and water resistivity and between subsurface resistivity and TDS

Well ID	Sampling (Month)	Ground water table depth referred from ground surface (m)	Water conductance $(\mu\Omega/cm)$	Soil conductance $(\mu\Omega/cm)$	Water resistivity (Ω.m)	Subsurface resistivity (Ω.m)	Measured TDS (mg/L)
MW3	Aug-09	0.942	35240	9083	0.2838	1.101	21410
MW5	Aug-09	1.070	33280	9497	0.3005	1.053	20330
MW6	Aug-09	0.944	14870	3211	0.6725	3.114	8940
MW7	Aug-09	1.496	35270	10384	0.2835	0.963	21190
MW8	Aug-09	0.999	23010	5173	0.4346	1.933	13810
MW10	Aug-09	1.135	34650	18904	0.2886	0.529	21060
MW11	Aug-09	1.150	27250	8197	0.3670	1.22	9280
MW12	Aug-09	0.738	12620	2289	0.7924	4.368	7660
MW3	Nov-09	0.964	34420	11099	0.2905	0.901	21090
MW4	Nov-09	1.025	34710	11614	0.2881	0.861	21420
MW6	Nov-09	0.770	15790	3212	0.6333	3.113	9750
MW7	Nov-09	1.560	34720	9785	0.2880	1.022	21480
MW8	Nov-09	1.014	29121	6954	0.3434	1.438	18050
MW10	Nov-09	1.160	33930	13850	0.2947	0.722	20690
MW11	Nov-09	1.516	25920	9524	0.3858	1.05	8900
MW3	Feb-10	1.117	36890	11905	0.2711	0.84	21680
MW4	Feb-10	1.226	33030	14045	0.3028	0.712	19430
MW5	Feb-10	1.277	37990	13908	0.2632	0.719	22350
MW6	Feb-10	1.061	17581	3591	0.5688	2.785	10340
MW7	Feb-10	1.772	38640	24450	0.2588	0.409	22800
MW10	Feb-10	1.386	39380	18051	0.2539	0.554	23250
MW11	Feb-10	1.983	35842	16694	0.2790	0.599	9820
MW12	Feb-10	1.021	15731	3724	0.6357	2.685	9220

Water resistivity was plotted as a function of subsurface resistivity (Figure 5.21). The best regression line between subsurface resistivity and water resistivity indicated the following empirical relationship:

$$\rho_e = 6.4708\rho_w - 1.0488, \tag{5.1}$$

Where ρ_e is the subsurface resistivity and ρ_w is the water resistivity in Ω.m.

Both parameters showed good correlations (R^2 = 0.959). The analyses reaffirmed the basis for using subsurface resistivity in studying the salinity distribution in the groundwater system of Carey Island. This finding revealed that the subsurface resistivity of a Quaternary alluvium aquifer (comprising dominantly coarse, medium, and fine sand, as well as some gravel) and of saturated groundwater both affected salinity.

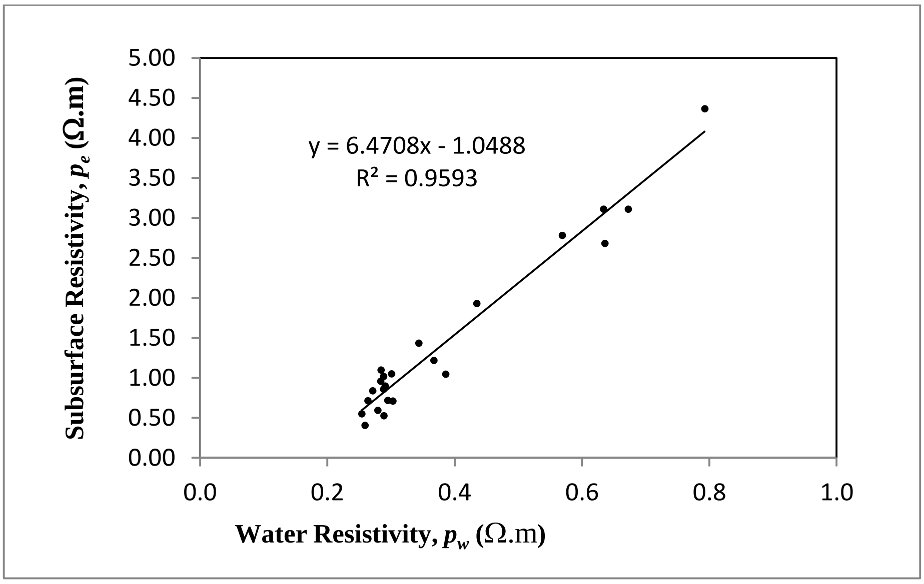

Figure 5.21: Subsurface resistivity versus water resistivity. Both parameters showed good correlations with R^2 = 0.959

TDS and subsurface resistivity were also plotted (Figure 5.22). Both parameters showed good correlations (R^2 = 0.932). The best regression line of the plot indicated the following empirical relationship:

$$\log TDS = -0.1411\rho_e + 4.4286. \qquad (5.2)$$

In this study, an empirical relationship between TDS and subsurface resistivity has been obtained [(Equation (5.2)], by which three TDS-based groundwater salinity degrees could be identified following the classification by Fetter (2002). Inserting the TDS-based groundwater salinity degree values into Equation (5.2), the resistivity values were acquired, from which the groundwater salinity degree were determined according to the set colour coding with the designated range of resistivity values. The results obtained were as follows: fresh water (ρ_e>10.0 Ω.m); brackish water (3.0 Ω-m<ρ_e< 10.0 Ω.m), and saline water (ρ_e< 3.0 Ω.m). Three colour codes (blue, green, and red) were used to denote the different groundwater salinity degree (respectively freshwater, brackish water, and saline water) as apparent in the resistivity image.

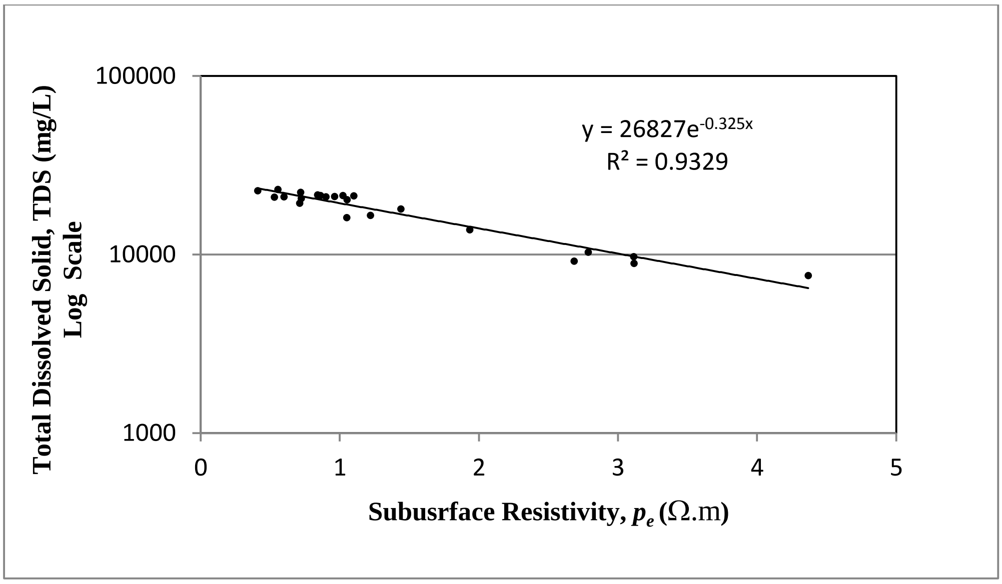

Figure 5.22: Subsurface resistivity versus TDS. Both parameters showed good correlations with R^2 = 0.932

The TDS was plotted against water specific conductance, σ_w (in µΩ.cm) as well, as shown in Figure 5.23. Both parameters showed good correlations (R^2 = 0.994). The fitted line revealed the following empirical relationship:

$$\mathrm{TDS} = 0.5958\sigma_{\mathrm{w}} + 203.71. \qquad (5.3)$$

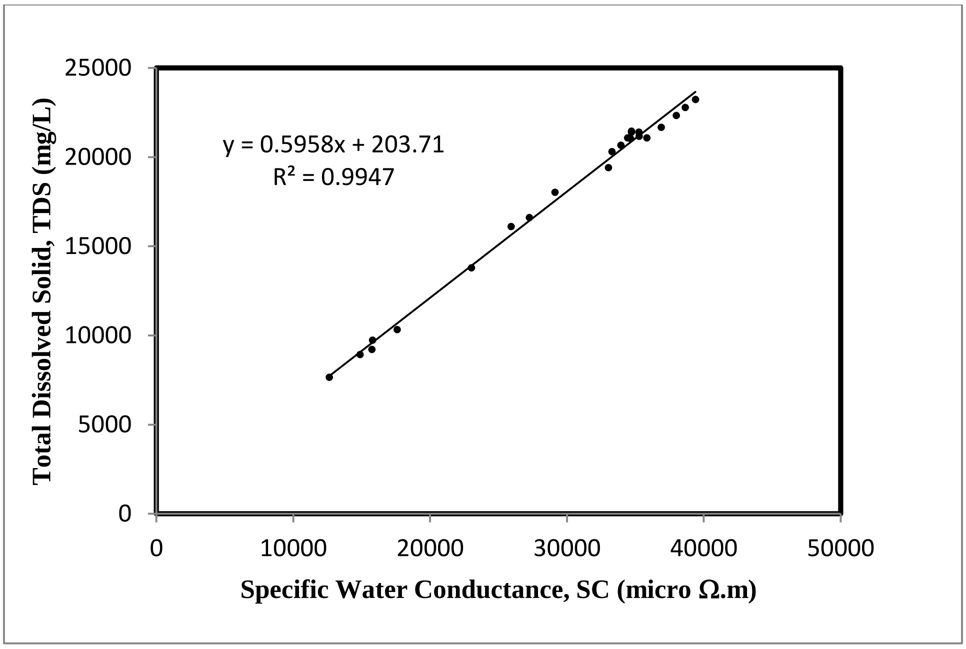

Figure 5.23: TDS versus specific water conductance. Both parameters showed good correlations (R^2 = 0.994).

The relationship of formation resistivity to fluid conductivity depends on the sediment type and pore-water conductivity. The linear formation ρ_f(Ω.m) and pore-water resistivity ρ_w(Ω.m) can relate in terms of the electrical conductivities σ_w and σ_f (S/m) (Archie, 1942), as follows:

$$\sigma_w = F\sigma_f, \qquad (5.4)$$

where the proportionality constant F is the "formation factor" related to sediment porosity. Equation (5.4) is valid for sediments which matrix resistivity is high and the main conductor is pore water. A significant amount of clay in soil sediment can be a significant conductor (Poulsen et al., 2010). Consequently, formation resistivity becomes a non-linear function of pore-water conductivity, especially in freshwater with conductivities less than 0.5 S/m. Therefore, the linear correlation between TDS and subsurface resistivity cannot be used directly for semi-confined aquifer that contain thick marine clay layer.

The relationship between subsurface resistivity and TDS data derived from Equation (5.2) was used for the unconfined aquifer system containing granular material saturated with water. For MW3 and MW4 located in the semi-confined, the sub-surface profile showed a marine clay layer with a thickness of 30 m from the ground level. However, the correlation between subsurface resistivity and TDS data could be applied in the semi-confined aquifer at water-saturated sandy soil layer. The screen depth (depth where groundwater samples taken) was at the sand layer of the first aquifer in the semi-confined zone. The screen for MW3 was located at a depth of 46 to 48 m, whereas that for MW4 was placed at 34 to 36 m. According to Baba (2003), the screen depths were located at the Gula Formation where the formation was as deep as 54 m in Carey Island. The properties of the sand material were assumed to be similar with the properties of the Gula Formation in the unconfined aquifer system. Equation (5.2) can only be used in depths ranging from 30–54 m, which is still in the Gula Formation.

5.4 Field calibration

The field calibration was done to find the relationship between subsurface resistivity values with various concentration of pore fluid on the sandy material. Soil samplings were conducted inland about 20 m away from the coast to avoid maximum high tide. Sieve analyses for two samples in Figure 5.24 showed homogenous sand. The sieve-analysis curves almost identical with those for MW12 samples.

The result of resistivity values of materials and various concentrations of pore fluids is shown in Table 5.2. Correlation between both parameters as shown in Figure 5.25 with R^2 = 0.9765 revealing almost-linear correlation between pore-water conductivity and clean sand as mentioned by Archie (1942).

Resistivity differed slightly especially with TDS values 1,000 mg/L (maximum limit of freshwater) and 10,000 mg/L (level of saline water). For 1,000 mg/L TDS, subsurface resistivity for field calibration and inversion model were 10.1 Ω.m and 10.0 Ω.m, respectively. For 10,000 mg/L TDS, subsurface resistivity was 2.9 Ω.m in field calibration and 3.0 Ω.m for inversion model. The results showed slightly different values between field calibration and inversion models. The results confirmed correlation of subsurface resistivity from inversion model with TDS values can be used for determining groundwater salinity in unconfined groundwater system at Carey Island.

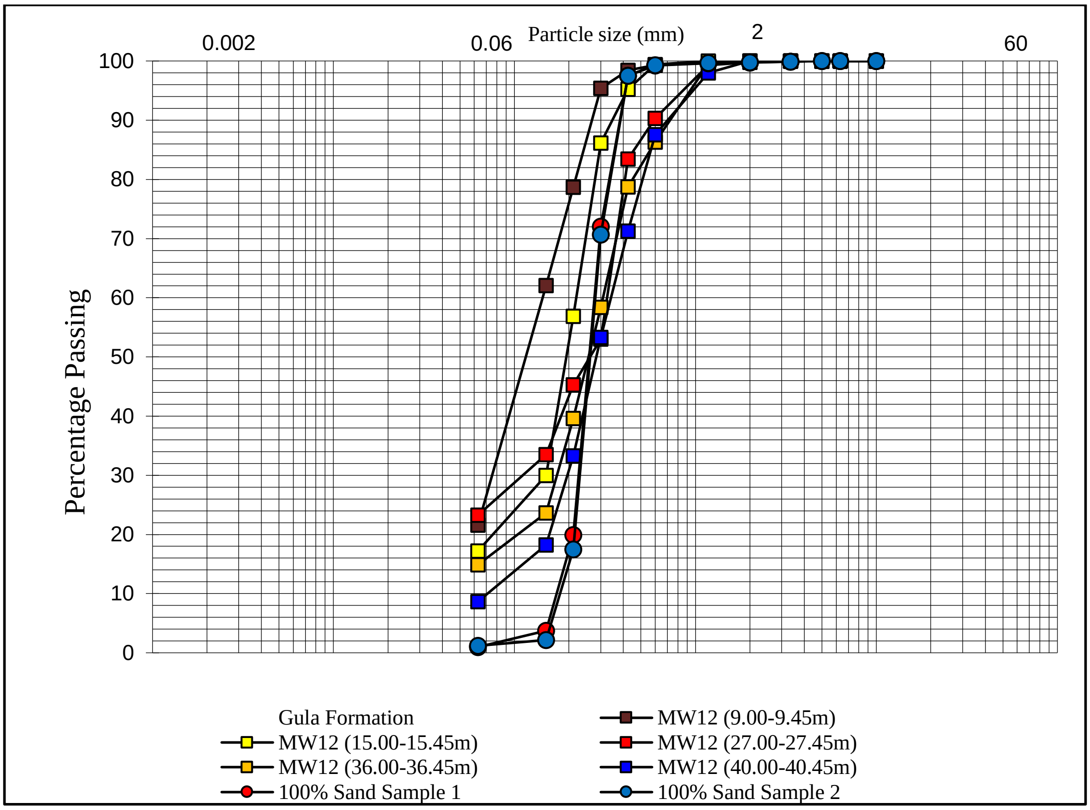

Figure 5.24: Analysis showing grain size in fine clean sand experiments near MW7 being almost identical with MW12 grain size

Table 5.2: TDS and resistivity value for various different material types

Material	TDS (mg/L)	Resistivity Value (Ω.m)
Rain Water	518	6.705
Sea Water	26000	0.292
Dry Sand	-	445
Saturated Sand	26000	0.735
Saturated Sand	23000	0.813
Saturated Sand	20000	1.082
Saturated Sand	17000	1.572
Saturated Sand	15000	1.625
Saturated Sand	13000	1.792
Saturated Sand	10000	2.951
Saturated Sand	7000	3.124
Saturated Sand	5000	4.712
Saturated Sand	3000	6.115
Saturated Sand	2000	7.615
Saturated Sand	1000	9.432
Saturated Sand	500	13.446

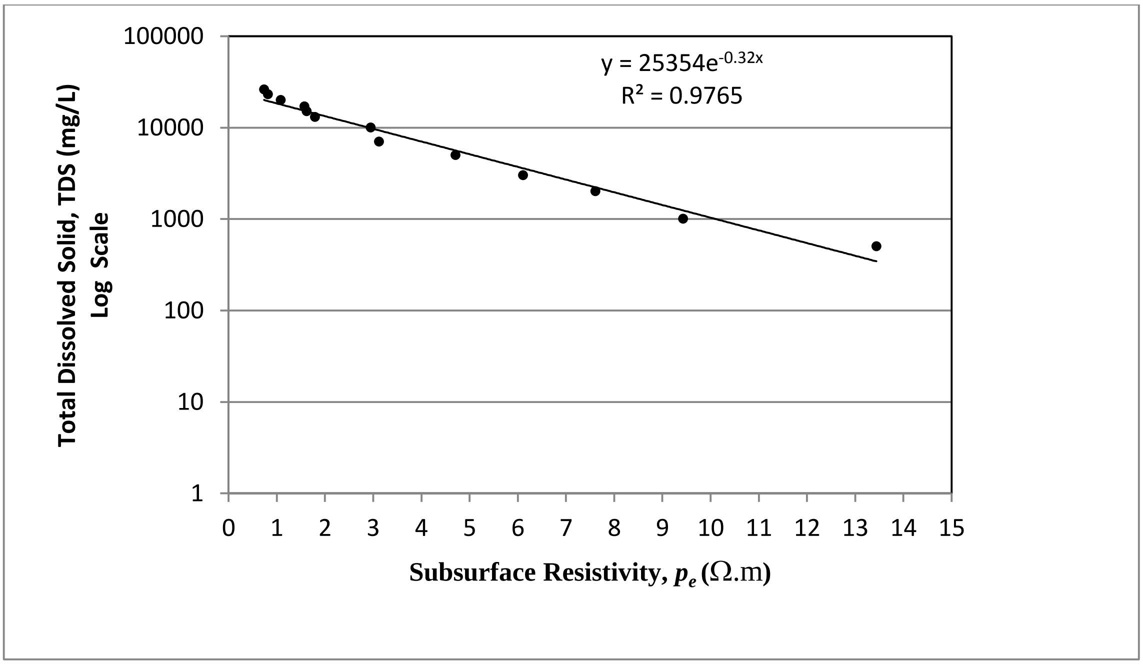

Figure 5.25: Subsurface resistivity versus TDS in field calibration

5.5 Time-Lapse Electrical Tomography (TLERT) measurement results

TLERT was conducted to investigate the changes of the subsurface resistivity due to salinity changes in groundwater aquifer by tides. The measurements involved six survey lines crossing over MW7, MW10, MW11 and MW12. This section showed two examples of TLERT measurements for MW12 in August 2009 (Figures 5.26 until 5.30) and February 2010 (Figures 5.31 until 5.35). The measurement conducted in August 2009 which was a wet season with the average monthly rainfall of 280 mm whereas in February 2010 was a dry season with the average monthly rainfall of 50 mm (Table 4.1).

The TLERT measurement result for survey line crossing over MW12 at the beginning of the investigation in August 2009 is shown in Figure 5.26(a), (b) and (c).The percent change of MW12’s resistivity image [Figure 5.26(c)] was calculated using Equation (3.6). The percentage change of resistivity image was obtained from the comparison of the inversion model’s subsurface resistivity, which was obtained from inversion results at the second time [Figure 5.26 (b)]. The initial inversion results measured as a reference model resistivity in the first time [Figure 5.26(a)]. The second-time inversion result was obtained after one hour of measuring the reference model’s resistivity. The other inversion results measured for third, fourth, fifth and sixth times [Figures 5.27(a), 5.28(a), 5.29(a) and 5.30 (a)] also referred to the initial inversion result [Figure 5.26(a)]. Percentage resistivity changes were calculated between the reference model [Figure 5.26(a)] and the inversion results [Figures 5.26(b), 5.27(a), 5.28(a), 5.29(a) and 5.30(a)] using equation (3.6). Resistivity percentage changes for the reference model resistivity of MW12 in August showed (-) 45.61(minimum values) to (+) 127.75 (maximum values) in the six hours interval of the TLERT measurement.

The positive percentage value showed dominancy in the percentage resistivity changes image [Figures 5.26(c), 5.27(b), 5.28(b), 5.29(b) and 5.30(b)] at the interval between

11.00a.m. to 5.00p.m. The TLERT measurements between 11.00 a.m. and 5.00 p.m. (Figures 5.26, 5.27, 5.28, 5.29 and 5.30) were conducted when low tides were occurring. The positive percentage showed a high resistivity value compared to the initial reference model for the same area where the TLERT measurement was conducted. The positive percentage showed low ion concentration in the pore fluids compared to the initial resistivity measurement. A low ion concentration was due to the movement of the high concentration ions in one hour interval from inland area toward to coastal area during low tide condition. The movement of the ion concentration was contributed by the difference in the level between the seawater during tide condition and groundwater in the aquifer. The mixture of the pore fluid with surface water recharge also contributed to the reduction of the ion concentration especially in the shallow aquifer. Nevertheless, the reduction of the ion concentration did not change the water type of the aquifer as a whole. The saline water zone could still be seen at the average depth of 30 m from ground level (Figures 5.26, 5.27, 5.28, 5.29 and 5.30).

The final reading at 5.00 p.m. (sixth time) showed dominancy of negative percentage with the value of (-) 40% [Figure 5.30(b)]. This negative percentage value was contributed by the high tide which occurred for 2 hours. The negative percentage showed that the zone had a low resistivity value compared to the initial reference model. The pore fluid in the groundwater aquifer had an increase in the ion concentration through the seawater intrusion from the high tide condition that resulted in the low resistivity value.

TLERT studies continued in February (minimum rainfall), at the same line position in August (maximum rainfall). Inversion-model data as reference model were obtained at one hour intervals from the beginning of high tide [Figure 5.31(a)]. Percentages of resistivity change [Figure 5.31(c)] were obtained by comparing series of inversion data [Figure 5.31(b)] with the reference model. The others inversion results series measured

[Figures 5.32(a), 5.33(a), 5.34(a) and 5.35(a)] also referred to the initial result of reference model [Figure 5.31(a)]. The TLERT measurements were conducted at time 10.00 a.m until 4.00 p.m.

Range of resistivity change percentages is about (-) 48.52 to 55.08 in the six hours interval of the TLERT measurement [Figures 5.31(c), 5.32(b), 5.33(b), 5.34(b) and 5.35(b)]. Resistivity image for August 2009 (maximum rainfall) showed 35 m-thick aquifer-brackish-freshwater water lens, which was reduced to 25 m in February 2009 (minimum rainfall) (Figure 5.31). The decreased was caused by freshwater recharge (through infiltration of unconfined layer) being greater in the wet season.

Salinity-change trend at the bottom of the image for both conditions showed movement from right to left. The trend was believed to have been caused by incremental daily tide passing through the high hydraulic conductivity resulting from high porosity of the material in the studied area. For the rest of the TLERT measurement, inversion model and percentage resistivity changes images are enclosed in Appendix I. The summary of the percentage resistivity changes is showed in Table 5.3.

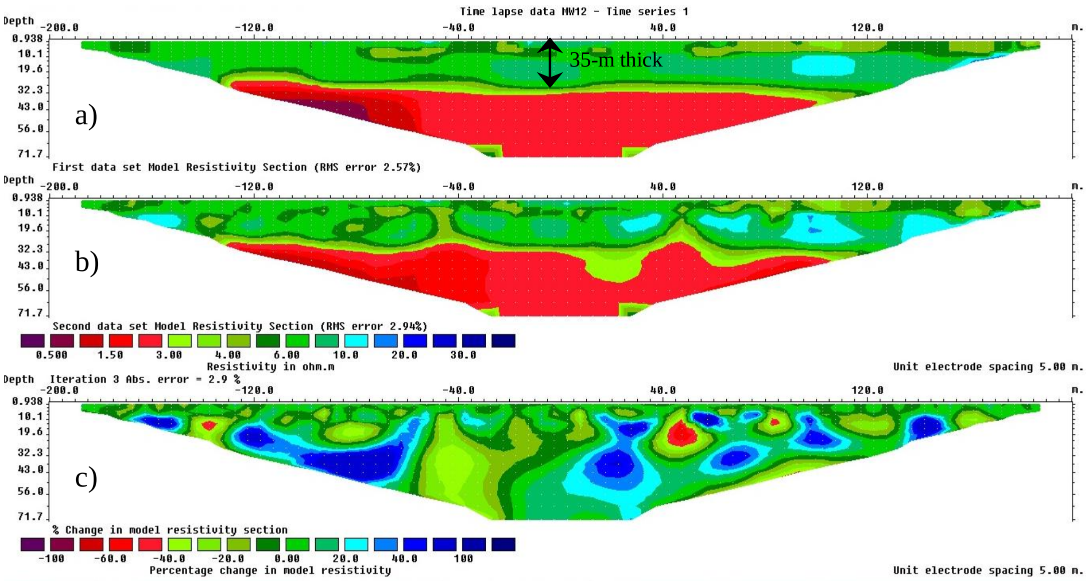

Figure 5.26: TLERT measurement results of MW12 at 11.00 a.m.–1.00 p.m.;26 August 2009;a) Inversion results in the first time as reference model at 11.00 a.m.-12.00 p.m., b) Inversion results in the second time at 12.00 p.m.-1.00 p.m., and c) MW12 resistivity change percentages

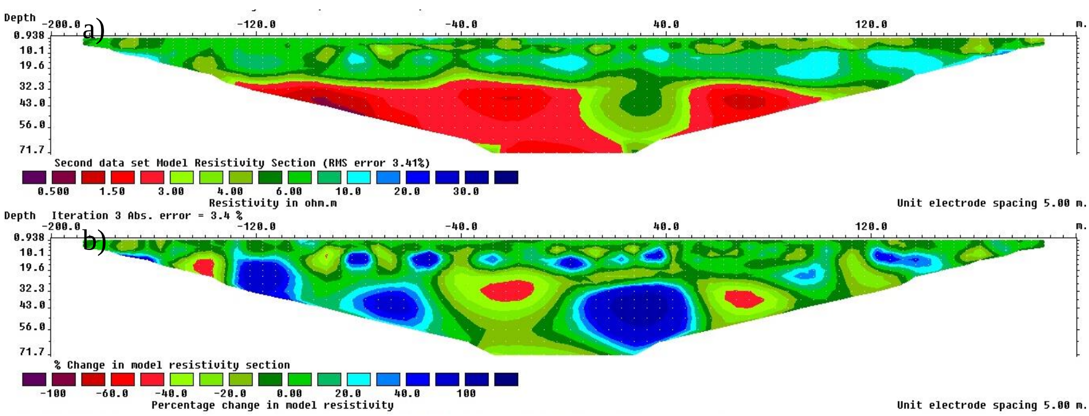

Figure 5.27: a) Inversion results in the third time at 1.00 p.m.-2.00 p.m., and b) MW12 resistivity change percentages

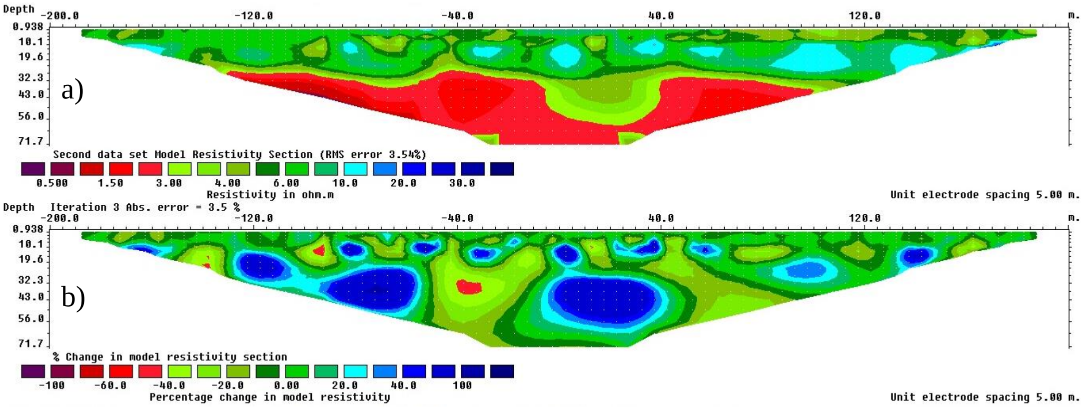

Figure 5.28: a) Inversion results in the fourth time at 2.00 p.m.-3.00 p.m., and b) MW12 resistivity change percentages

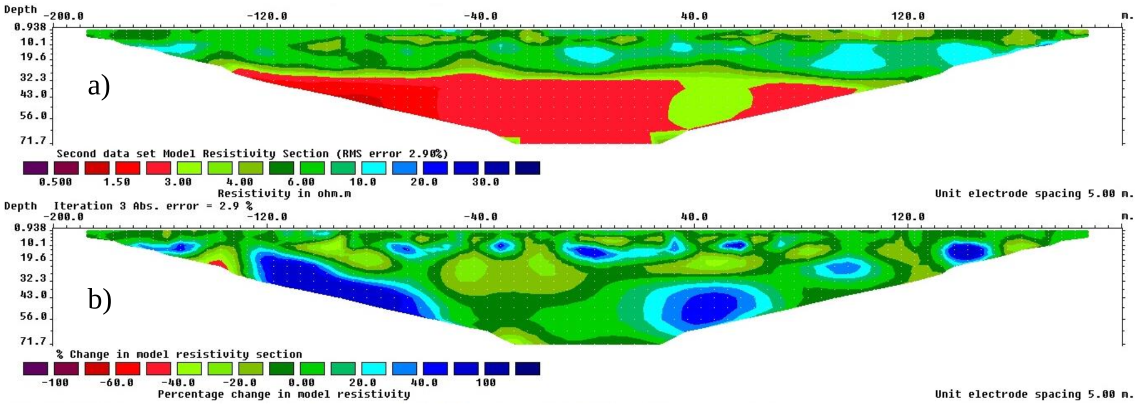

Figure 5.29: a) Inversion results in the fifth time at 3.00 p.m.-4.00 p.m., and b) MW12 resistivity change percentages

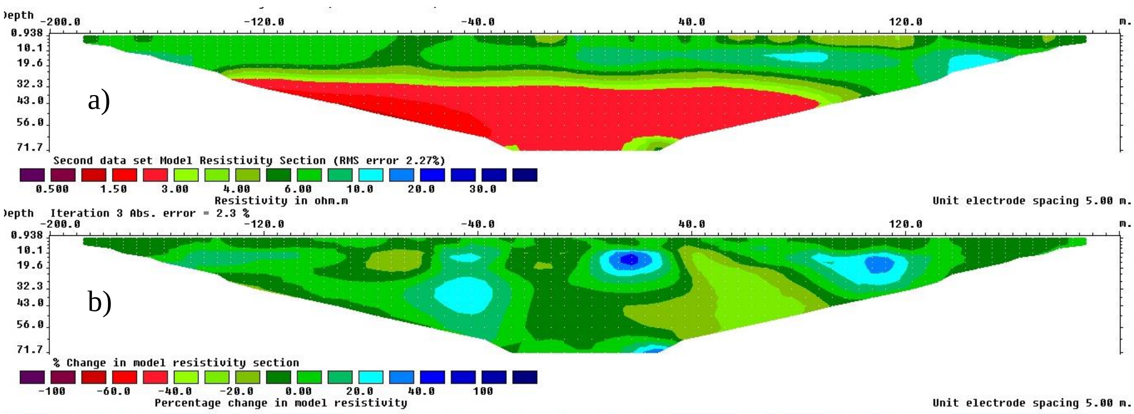

Figure 5.30: a) Inversion results in the sixth time at 4.00 p.m.-5.00 p.m., and b) MW12 resistivity change percentages

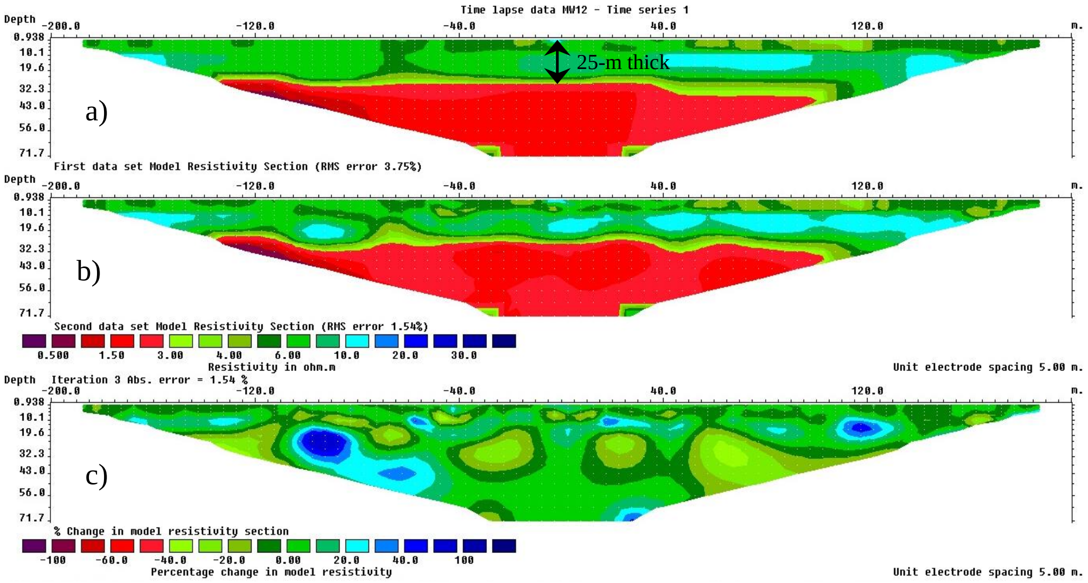

Figure 5.31: TLERT measurement results of MW12 at 10.00 a.m. - 12.00 a.m.; 10 February 2010; a) Inversion results in the first time as reference model at 10.00 a.m.-11.00 a.m., b) Inversion results in the second time at 11.00 a.m.-12.00 p.m., and c) MW12 resistivity change percentages

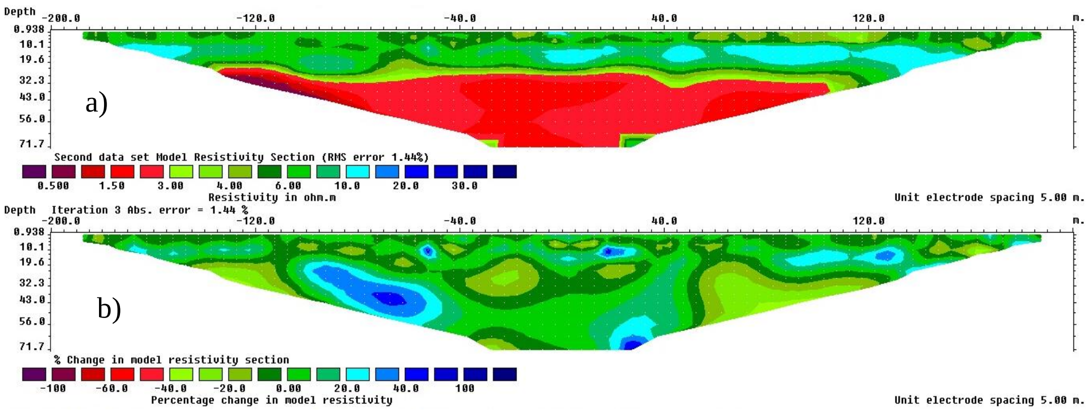

Figure 5.32: a) Inversion results in the third time at 12.00 p.m.-1.00 p.m., and b) MW12 resistivity change percentages

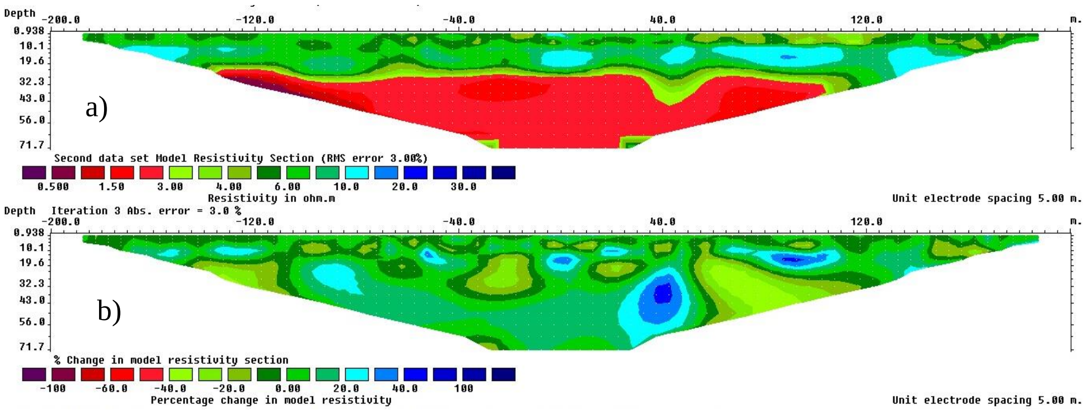

Figure 5.33: a) Inversion results in the fourth time at 1.00 p.m.-2.00 p.m., and b) MW12 resistivity change percentages

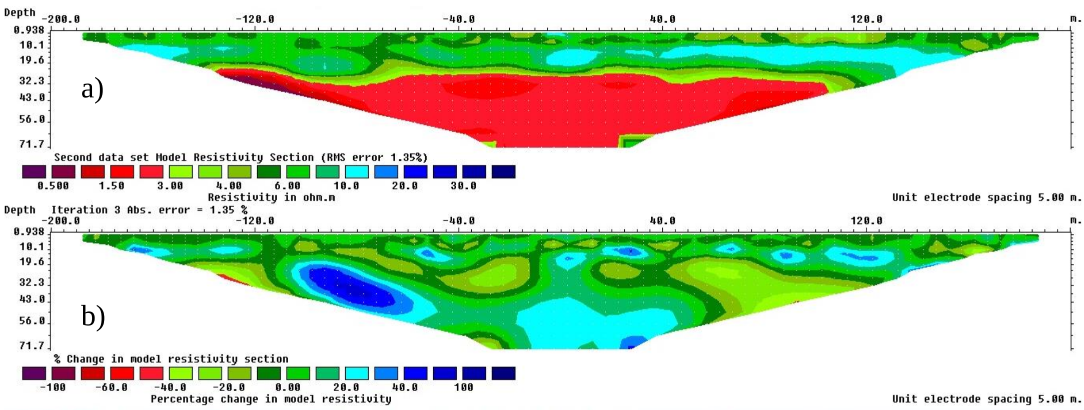

Figure 5.34: a) Inversion results in the fifth time at 2.00 p.m.-3.00 p.m., and b) MW12 resistivity change percentages

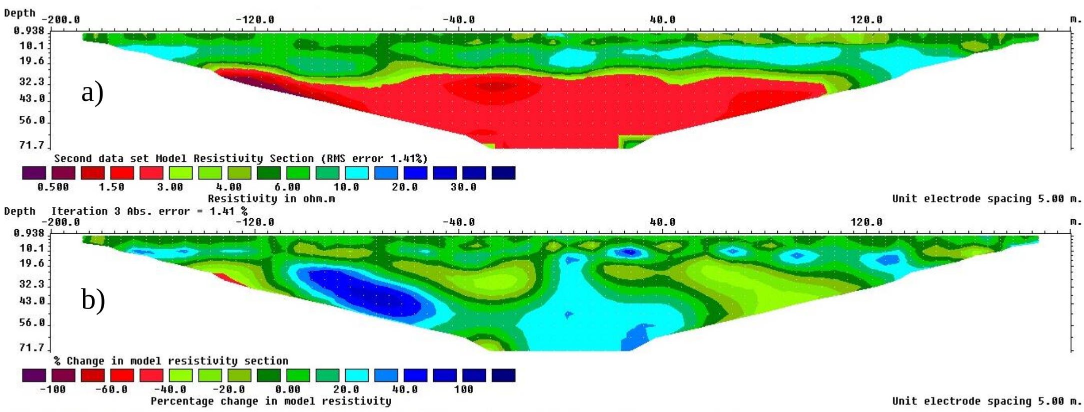

Figure 5.35: a) Inversion results in the sixth time at 3.00 p.m.-4.00 p.m., and b) MW12 resistivity change percentages

Table 5.3: Summaries of percentage change in model resistivity

MW ID	Date	Percentage change in model resistivity	
		Min Negative	Max Positive
MW7	28 August 2009	-58.90	284.19
MW10	22 November 2009	-53.70	93.35
MW10	12 August 2009	-53.01	103.08
MW11	27 November 2009	-61.31	116.16
MW12	26 August 2009	-45.61	127.75
MW12	10 February 2010	-48.52	55.08

5.6 Summary

Subsurface resistivity images obtained showed more than 80% have low resistivity (<3 Ω.m), except for the image that cross over MW6 and MW12. Previous studies indicated low resistivity value of less than 5 Ω.m was due to seawater intrusion.

In order to establish the empirical relationship between subsurface resistivity and the groundwater salinity in the study area, the subsurface resistivity results were correlated with TDS. The correlation results were used to derive the empirical equation for the groundwater salinity (fresh, brackish and saline) of sandy aquifer system in Carey Island.

The resistivity survey measurements and groundwater sampling from deep monitoring wells were conducted in three months times where twenty three data from subsurface resistivity and TDS were collected to establish the empirical relationship. In the statistical analysis, the subsurface resistivity, water resistivity and TDS data followed the normal distribution where the skewness and kurtosis value was nearly closed to -1 and +1. All the data showed strong linear relationships where Pearson correlation coefficient (r) showed value approaching -0.9 to +0.9. This can be used to derive a linear regression to determine the relationship between the data, especially subsurface resistivity versus water resistivity and subsurface resistivity versus TDS data. The plotted graph of the resistivity versus water resistivity and subsurface resistivity versus TDS showed R^2 value of 0.959 and 0.932 respectively that showed strong linear relationships.

The relationship derived from the empirical equation revealed that three types of groundwater salinity can be depicted in the resistivity images. The water types are fresh (ρ_e>10.0 Ω.m), brackish (3.0 Ω.m<ρ_e< 10.0 Ω.m), and saline (ρ_e< 3.0 Ω.m).

The correlation relationship between the subsurface resistivity and TDS data can be used to determine the distribution and location of the boundaries of freshwater, brackish and saline in the aquifer system. However, 2-D resistivity images only provide the subsurface resistivity image and groundwater salinity distribution in vertical profile view. Therefore, the relationship derived between subsurface resistivity and TDS will be used to plot the three dimensional (3-D) resistivity mapping. The relationship provided the distribution and location of the boundaries of water types in better view which covered the whole study area. The 3-D resistivity mappings results are discussed in Chapter 6.

The result of the TLERT measurement concluded that the tide conditions and recharge affected the groundwater salinity in the aquifer. The difference in the resistivity changes percentage with positive and negative value showed dynamic changes in the salinity of the groundwater aquifer happened every day. The TLERT results reaffirmed the source of salinity in groundwater aquifer of Carey Island was due to seawater intrusion which confirmed by the geochemistry analysis in section 4.4.